Exchange bias and interface electronic structure in Ni/Co_3O_4(011)

C. A. F. Vaz,[1,2,*] E. I. Altman,[3,2] and V. E. Henrich[1,2]
[1]*Department of Applied Physics, Yale University, New Haven, Connecticut 06520, USA*
[2]*Center for Research on Interface Structures and Phenomena (CRISP), Yale University, New Haven, Connecticut 06520, USA*
[3]*Department of Chemical Engineering, Yale University, New Haven, Connecticut 06520, USA*
(Received 21 January 2010; revised manuscript received 3 March 2010; published 30 March 2010)

A detailed study of the exchange-bias effect and the interfacial electronic structure in Ni/Co_3O_4(011) is reported. Large exchange anisotropies are observed at low temperatures, and the exchange-bias effect persists to temperatures well above the Néel temperature of bulk Co_3O_4, of about 40 K, to ~80 K for Ni films deposited on well-ordered cobalt oxide surfaces, and ~150 K for Ni films deposited on rougher Co_3O_4 surfaces. Photoelectron spectroscopy measurements as a function of Ni thickness show that Co reduction and Ni oxidation occur over an extended interfacial region. We conclude that the exchange bias observed in Ni/Co_3O_4, and in similar ferromagnetic metallic/Co_3O_4 systems, is not intrinsic to Co_3O_4 but rather due to the formation of CoO at the interface.

DOI: 10.1103/PhysRevB.81.104428 PACS number(s): 68.37.Og, 68.35.Ct, 68.37.Ps

I. INTRODUCTION

The exchange anisotropy, first reported by Meiklejohn and Bean[1] for surface-oxidized Co nanoparticles, is manifested by a horizontal shift in the hysteresis loop of magnetic systems in contact with an antiferromagnet, an interface phenomenon explained by exchange coupling between the spins at the interface between the two materials.[2] Although studied for many decades now, a full understanding of exchange bias at the microscopic level remains challenging,[3–9] largely because of the difficulty in resolving the interface spin and the electronic structure between the two materials. Several microscopic models have been proposed to explain the exchange anisotropy and the small exchange bias observed experimentally *vis à vis* the strength of the spin-spin exchange coupling. The latter effect is generally attributed to interface roughness, antiferromagnetic domains, and steps at the interface, which lead to a reduction in the effective exchange coupling.[3–11] Hence, a detailed knowledge of the interface structure is key to understanding the mechanisms responsible for the strength of the exchange anisotropy observed between different compounds.

Cobalt, like most 3*d* transition-metal elements, can exist in more than one oxidation state. Of the two stable cobalt oxides, the mixed-valence compound, $Co^{2+}Co_2^{3+}O_4$, crystallizes in the spinel structure, with a lattice constant of $a=8.086$ Å at room temperature[12] while the CoO phase crystallizes in the rocksalt structure ($a=4.260$ Å).[13] Both oxides are antiferromagnetic at low temperatures, with Néel temperatures of approximately 40 and 290 K, respectively.[14–21] While the critical temperature in these materials is too low for practical devices, their well-defined and localized spin structures make them model systems for the study of exchange anisotropy. In this context, our recent demonstration of the growth of high-quality crystalline Co_3O_4(011) thin films on $MgAl_2O_4$(011) substrates,[22] and the recent reports of enhanced temperatures for the onset of exchange bias in $Ni_{80}Fe_{20}/Co_3O_4$ heterostructures,[23–26] have motivated us to examine the exchange bias in well-characterized Co_3O_4(011) films, and to probe the electronic structure of the metal/Co_3O_4 interface. We chose Ni as the ferromagnetic layer in order to facilitate the electronic characterization of the interface. Ni has an oxygen affinity similar to that of Co,[27] and when exposed to air it forms a surface-oxide layer ~3 Å thick that acts as a passivation layer.[28–31] Here, we report the observation of large exchange bias in the Ni/Co_3O_4 system, which persists to temperatures well above the Néel temperature of Co_3O_4; the effect is stronger and extends to higher temperatures in systems exhibiting greater interface roughness. From photoelectron spectroscopy, we show that the deposition of the Ni layer leads to a reduction in the Co_3O_4 over a few atomic layers and to Ni oxidation at the interface between these materials. A CoO/NiO interfacial region is found to form between the Co_3O_4 and Ni films. Hence, we conclude that the observed exchange bias is not intrinsic to Co_3O_4 but instead to CoO, mediated by a NiO interfacial layer.

II. SAMPLE GROWTH

$MgAl_2O_4$(011) single crystals were used as substrates for the growth of Co_3O_4 because of the small lattice mismatch of −0.05% and good thermal and chemical stability. $MgAl_2O_4$ has the same crystal structure as Co_3O_4, which should preclude the formation of antiphase boundaries that originate when lower symmetry structures are grown on higher-symmetry surfaces. Also, the direction perpendicular to the (011) surface is characterized by having a repeat period of four atomic planes as opposed to the 8-period repeat along the [100] direction or the 18-period repeat of the [111] direction.[32] It therefore should be less susceptible to stacking faults and antiphase boundary formation, leading to fewer defects in the film.[22]

The samples in this study were grown by molecular-beam epitaxy in a dual ultrahigh vacuum (UHV) system comprising a growth chamber (base pressure $\sim 1\times 10^{-9}$ mbar) equipped with a reflection high-energy electron diffraction (RHEED) system, and an analysis chamber (base pressure $\sim 3\times 10^{-10}$ mbar) for low-energy electron diffraction (LEED), x-ray photoemission (XPS), and Auger-electron

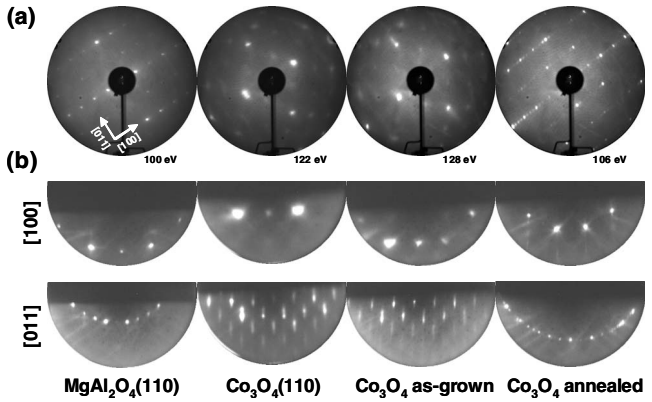

FIG. 1. (a) Low-energy electron-diffraction patterns of the $MgAl_2O_4$ and $Co_3O_4(011)$ films immediately after growth, and of the as-grown and annealed films before Ni deposition. The crystal orientation, inferred from the LEED pattern and confirmed by Laue diffraction, is shown in the inset. (b) Corresponding reflection high-energy electron-diffraction patterns, along different azimuths (parallel to the electron beam, set at a grazing angle of incidence). The electron-beam energy was 10 keV for the $MgAl_2O_4$ patterns and 11 keV for the Co_3O_4 patterns.

spectroscopy. The systems are interconnected by a gate valve, allowing sample transfer under UHV. In this work, the XPS spectra were obtained using the Mg $K\alpha$ line ($h\nu$ =1253.6 eV) of a double anode x-ray source and a double pass cylinder mirror analyzer (Φ 15–255 G) set at a pass energy of 25 eV (energy resolution of about 0.8 eV). Further *ex situ* characterization included x-ray diffraction and reflectometry (Cu $K\alpha$ line, using a Shidmazu diffractometer set in the parallel beam geometry) and superconducting quantum interference device magnetometry (Quantum Design). Several $Ni/Co_3O_4/MgAl_2O_4(011)$ samples were prepared and characterized for this study. In addition, two extra structures were grown: a $Ni/SiO_x/Si(111)$ film, to determine the presence of exchange bias due to Ni surface oxidation; and a Ni/CoO/MgO(001) sample, to obtain a CoO XPS spectrum and to determine the exchange anisotropy in Ni/CoO. The growth procedures are distinct for the different types of samples, as discussed in detail next.

The Co_3O_4 samples were grown using the procedure described in Ref. 22, with the substrate held at 570 K during growth. The high quality of the $MgAl_2O_4(011)$ surface crystallinity was confirmed by LEED and RHEED, which display patterns characteristic of highly ordered surfaces, as shown in Fig. 1. The nominal Co_3O_4 thickness values, in the 30–40 nm range, are found to be in good agreement with the values obtained from x-ray reflectivity measurements. LEED and RHEED patterns typical of the Co_3O_4 films after growth are shown in Fig. 1. Compared with the $MgAl_2O_4(011)$ LEED patterns, the diffraction spots of the as-grown Co_3O_4 film are much broader and the background is more intense, indicating that the as-grown Co_3O_4 films have a significant amount of surface disorder. The RHEED patterns exhibit streaky and relatively broad diffraction spots, characteristic of a three-dimensional growth mode. However, along the [100] direction, the diffraction spots are found to lie in a Laue arc, indicative of a relatively smooth surface; this is in agreement with earlier results showing a unidirectional surface roughness morphology along this direction, with an average surface roughness of $\sim 2-3$ nm as determined from atomic force microscopy and transmission electron microscopy.[22] After the Co_3O_4 growth and *in situ* characterization, the sample was cleaved *ex situ*; one half was then annealed at atmospheric pressure in flowing O_2 (900 scc/min) at 820 K for 12 h; this temperature and oxygen pressure favor the formation of Co_3O_4 over CoO.[33–35] Both as-grown and annealed samples were then returned to the growth system for Ni deposition. The Co_3O_4 films were first cleaned in an O plasma at 770 K for 30 min, and in one instance cooled to below 370 K under the O plasma. The surfaces of both as-grown and annealed films were then characterized *in situ* prior to the Ni film deposition; the corresponding diffraction patterns are labeled in Fig. 1 as "as-grown" and "annealed."

The annealing process induces significant transformations in the film surface structure, as shown by different and much sharper LEED and RHEED patterns in Fig. 1. In one instance, we observe the presence of a (4×1) surface reconstruction along the [100] direction, which we relate to the particular surface treatment during the O-plasma cleaning procedure, i.e., cooling below 370 K in O plasma [only (1×1) patterns were observed previously]. One possible explanation is the presence of adsorbed oxygen. Monitoring the LEED pattern evolution with increasing sample temperature in UHV (3×10^{-10} mbar) shows no changes in the LEED pattern up to 570 K; no changes in the XPS spectra are found after this process, indicating that the Co_3O_4 films are stable in UHV up to that temperature. The related $Fe_3O_4(110)$ surface has been found to reconstruct in a (3×1) structure[36–38] while a (4×1) reconstruction has been found for the (001) surface;[39,40] this extra periodicity in the lattice has been attributed to the presence of Mg or Ca surface impurities that have migrated from the bulk or from the substrate upon annealing.[38–40] Although no impurities were detected in the XPS survey scans, a more detailed study is required before ruling out the effect of impurities as the origin of the observed surface reconstruction. One striking feature of the LEED patterns is the different symmetry exhibited by the as-grown and annealed films: while the former exhibit an oblique unit cell, the latter are found to exhibit a rectangular unit cell. The LEED patterns are compatible with the two possible bulk terminations of the (011) plane of the spinel structure: type A for the annealed films, with a $Co_2^{2+}Co_2^{3+}O_4$ nominal stoichiometry exhibiting a rectangular unit cell, and type B for the as-grown films, with a $Co_2^{3+}O_4$ nominal stoichiometry and an oblique unit cell.[22] The XPS spectra of both as-grown and annealed films are identical and characteristic of Co_3O_4.

The Ni deposition (from an effusion cell) was carried out with the substrate held at ambient temperature; the system pressure during evaporation was 1×10^{-7} mbar, with an evaporation rate ~1 Å/min. We find that the Ni film grows single crystalline, albeit with very broad RHEED patterns, as shown in Fig. 2(a), that indicate a large density of crystalline imperfections (surface roughness and/or mosaicity), with $Co_3O_4(011)[111]\|Ni(011)[100]$ [Fig. 2(b)] or the twin orientation $Co_3O_4(011)[1\bar{1}\bar{1}]\|Ni(011)[100]$. The above rela-

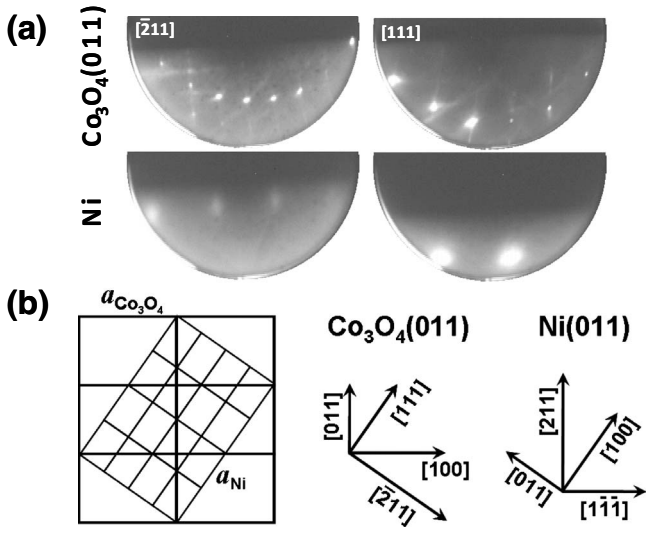

FIG. 2. (a) Co_3O_4 and Ni RHEED patterns along the [111] and [$\bar{2}$11] azimuths of the annealed Co_3O_4(011) film (at 11 keV incident electron-beam energy). (b) Schematic of the epitaxial relationship between [110]-oriented Ni and Co_3O_4.

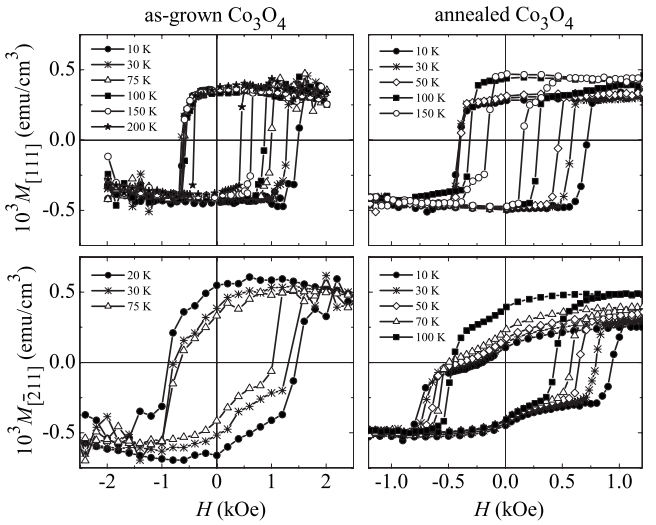

FIG. 3. Magnetization (M) versus magnetic field (H) characteristics for the Ni film deposited on the as-grown (left) and annealed (right) Co_3O_4 films for fields applied along the [111] (top) and [$\bar{2}$11] (bottom) directions of Co_3O_4(011).

tionship gives $\sqrt{3}a_{Co_3O_4}=3.97a_{Ni}$, where $a_{Ni}=3.5241$ Å is the lattice parameter of fcc Ni,[41] corresponding to a lattice misfit of −0.65%. The XPS measurements show Ni 2p peaks typical of metallic Ni; trace amounts of O were detected in the Ni film, as indicated by a small O 1s peak. To study the evolution in the electronic structure at the Ni/Co_3O_4 interface, a separate study was carried out where the XPS spectra were recorded as progressively more Ni (0, 1.8, 5.3, 14, and 80 Å) was added to a 30-nm-thick Co_3O_4 film. In this case, the Ni film was deposited immediately after the Co_3O_4 growth.

Additionally, two control samples were grown, one consisting of an 8-nm-thick Ni film grown on the native oxide layer of a Si(111) wafer, and an 8 nm Ni/36 nm CoO/MgO(001) structure. For the latter sample, the MgO(001) single crystal was outgassed and cleaned *in situ* with an O plasma at 570 K for 30 min. Cobalt evaporation was carried out under an O_2 partial pressure of 1×10^{-5} mbar. This leads to single crystalline CoO(001), with good RHEED and LEED patterns (not shown) and with the correct stoichiometry, as determined by XPS (see Fig. 5 below). X-ray diffraction measurements confirm the presence of the [001]-oriented CoO phase, with an out-of-plane lattice constant $a_\perp=4.28$ Å, showing that the film is under compressive strain. The in-plane strain can then be estimated as $\epsilon_\parallel=-\epsilon_\perp c_{11}/(2c_{12})=-0.42\%$, where $c_{11}=260$ GPa and $c_{12}=145$ GPa are the elastic constants of CoO,[42] and $\epsilon_\perp=(a_\perp-a)/a$, where a is the equilibrium lattice constant. The misfit strain between CoO/MgO is $\eta=-1.31\%$, showing that the CoO film is partially relaxed.

III. RESULTS AND DISCUSSION

For the magnetic characterization, the samples were cooled from room temperature to 10 K under a magnetic field of −50 kOe, and magnetic hysteresis (M-H) curves were measured at increasing temperatures in fields up to ±3 kOe. The magnetic field was cycled once between the field range of the hysteresis measurements at 10 K to reduce training effects (observed for the first field cycle). For the Ni/Si(111) control sample, no shift in the M-H curve is observed down to 10 K, ruling out the presence of exchange bias arising from surface Ni oxidation (in agreement with the weak exchange bias in NiO, attributed to its low magnetocrystalline anisotropy).[3,4] The magnetic measurements were performed on several sets of samples and yielded consistent results; in the following, we present the results for the sample set whose LEED and RHEED patterns are shown in Fig. 1. The direction of the applied magnetic field was along the [111] and the [$\bar{2}$11] directions of the Co_3O_4(011) (the crystal orientation was confirmed by Laue diffraction). Representative magnetic hysteresis curves for the as-grown and annealed Co_3O_4 films along these two directions are shown in Fig. 3.

Several observations are pertinent: (i) a large shift is present in the M-H curves in both the as-grown and annealed Co_3O_4 samples (exchange anisotropy), being significantly larger for the as-grown samples by about a factor of 2 (e.g., 880 Oe for the as-grown sample at 10 K compared to 400 Oe for the annealed sample); (ii) the exchange anisotropy is present at temperatures well above the Néel temperature of Co_3O_4, with the as-grown films exhibiting exchange bias up to higher temperatures than the annealed films; (iii) a strong directional dependence of the shape of the hysteresis curves is found, which is distinct for the as-grown and annealed samples, and which persists at temperatures above which no shift in the curves is observed, indicating that it originates from magnetic anisotropies in the Ni film; and (iv) for the annealed samples, the magnetization at positive fields does not reach saturation when exchange anisotropy is present. The saturation magnetization of the Ni films, $M_{Ni}\sim500$ emu/cm^3, is close to the bulk value of

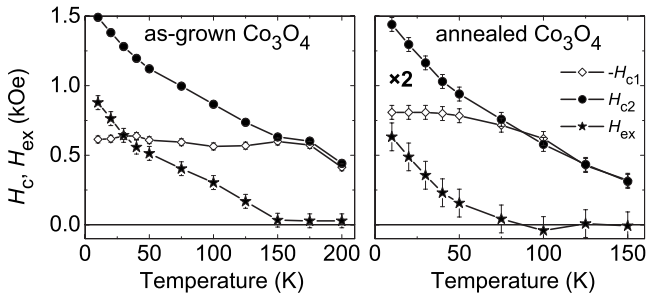

FIG. 4. Variation in the coercive field (H_c) and exchange anisotropy (H_{ex}) for the as-grown and the annealed $Co_3O_4(011)$ films along the [111] direction. The data on the graph on the right have been multiplied by a factor of 2.

510 emu/cm^3.[43] The variation in the coercive field and exchange bias as a function of temperature for the as-grown and annealed Co_3O_4 films along the [111] direction are plotted in Fig. 4, showing that the exchange bias sets in at around 80 K for the annealed films, and at around 150 K for the as-grown films. This result shows that the surface morphology of the Co_3O_4 film has a significant influence on the exchange anisotropy, acting to enhance it. Such an effect has been observed for single crystalline antiferromagnetic systems.[3,4,44] The interface energy, given by $\Delta E = M_{Ni} t_{Ni} H_{ex}$, where t_{Ni} is the Ni film thickness and H_{ex} is the exchange bias field, is ~ 0.35 erg/cm^2 for the as-grown sample and ~ 0.13 erg/cm^2 for the annealed sample at 10 K; these values are large in comparison with those typical for antiferromagnetic films.[4]

The presence of a strong uniaxial magnetic anisotropy in the Ni film agrees with the observation in RHEED and LEED of a [011]-oriented Ni film grown on annealed Co_3O_4. The magnetization lies in-plane, with the easy magnetization axis along the $Co_3O_4(011)[100]$ direction, which coincides with the [111] direction of Ni(011); this is also the easy magnetization direction of bulk fcc Ni.[43] However, the Ni[100] direction, which is a hard magnetization axis in bulk Ni, is a relatively easy magnetization direction in the Ni films while the Ni[110] direction is a hard axis. We attribute this behavior to a magnetoelastic contribution to the magnetic anisotropy arising from epitaxial strain in the Ni film. This energy contribution can be calculated within the linear theory of elasticity, giving $E_{me} = B\epsilon_{11} \sin^2 \theta$ to leading order, where ϵ_{11} is the in-plane strain, θ is the angle of the in-plane magnetization vector with respect to the Ni[100] direction, and B is the effective magnetoelastic coupling coefficient given by

$$B = \frac{3}{2}[(c_{11} - c_{12})\lambda_{100} + c_{44}\lambda_{111}]\frac{c_{11} + 2c_{12}}{c_{11} + c_{12} + 2c_{44}}, \qquad (1)$$

where c and λ are the elastic and magnetostriction coefficients, respectively. [This expression differs from that given by Kuriki[45–47] in that we constrain the magnetization to lie in the (011) plane.] Using the tabulated values of $c_{11}=2.481$, $c_{12}=1.549$, $c_{44}=1.242$ (units of 10^{12} dyne/cm^2),[48] $\lambda_{100} = -65.3 \times 10^{-6}$, $\lambda_{111} = -27.7 \times 10^{-6}$ (Ref. 49), one obtains $B = -1.22 \times 10^8$ erg/cm^3. For a fully strained Ni film ($\epsilon_{11} = -0.65\%$), the resulting magnetoelastic anisotropy is $K_{me} = +8.0 \times 10^5$ erg/cm^3; for comparison, the bulk magnetocrystalline anisotropy of Ni is[43] $K_1 = -5.6 \times 10^4$ erg/cm^3. Since we expect the Ni film to be partially relaxed, the magnetoelastic energy is likely to be comparable to the intrinsic magnetocrystalline anisotropy. Importantly, the sign of K_{me} favors $\theta = 0$, i.e., the magnetization pointing along the Ni[100] direction, which agrees with the data shown in Fig. 3. The magnetic switching behavior can then be understood in terms of the local energy minima present in the Ni(011) plane. In particular, the fact that the magnetization does not reach saturation at positive fields in the annealed Co_3O_4 films is explained by the switching of the magnetization from the Ni[$\bar{1}$00] direction (parallel to the applied magnetic field and to the exchange bias direction) to a direction near Ni[111], which gives a magnetization projection along the magnetic field of $\sim \cos(54.7°) = 1/\sqrt{3} = 0.58$. For the as-grown Co_3O_4 samples, an additional magnetic anisotropy contribution arises from the presence of a directional roughness via magnetic dipolar interaction (shape anisotropy).[50–56] The observed coercive fields are large (and larger for the as-grown Co_3O_4 film), suggesting the presence of strong pinning due to epitaxial strain fields or to exchange coupling with the antiferromagnetic spins. Magnetic measurements on the Ni/CoO(001) control sample show the presence of exchange bias at 20 K of 150 Oe, much smaller in magnitude than that observed in the Ni/Co_3O_4 system at that temperature; no exchange bias was present at 250 K.

The observation of exchange bias in Ni/Co_3O_4 is consistent with recent reports showing the presence of exchange bias up to 150 K in ion-beam-deposited $Ni_{80}Fe_{20}/Co_3O_4$ heterostructures[23–26] and up to 240 K in Co/Co_3O_4 bilayers grown by rf sputtering.[57–59] While in the latter studies the authors find an extended CoO interfacial region which is responsible for the observed temperature dependence of the exchange bias, the former reports suggest the presence of the Co_3O_4 phase only, from transmission electron microscopy and x-ray diffraction data. Since Ni and Co have similar oxygen affinities, a similar interface structure is expected for Co, Ni, or $Ni_{80}Fe_{20}$ films in contact with Co_3O_4. Therefore, to investigate if the enhanced exchange-bias effect is intrinsic to the Co_3O_4 film or due to modifications in the interface structure, we carried out a detailed spectroscopic characterization of the interface by studying the evolution of the x-ray photoemission spectra as a function of the Ni film thickness. These data are plotted in Fig. 5, where we also show the CoO spectra acquired from the Ni/CoO(001) sample. Corrections to the data include a five-point adjacent smoothing and satellite correction; energy shifts due to charging were corrected by aligning the O 1s peak to the tabulated value of 529.4 eV for Co_3O_4,[60–62] which is approximately the same for CoO,[61,63] NiO,[64] and $NiFe_2O_4$.[65,66] The O 1s peak decreases in amplitude with increasing Ni thickness, as expected; a small shoulder at higher binding energies is present in the Co_3O_4 and the 1.8–14 Å Ni films but is absent in the CoO spectrum; for the 80 Å Ni film, the O 1s line lies at the energy corresponding to the shoulder in the Co_3O_4 film, and is therefore likely to have the same origin. The presence of such a shoulder in the O 1s line is attributed to adsorbed O,[60,61,67–72] although we cannot rule out the presence of ad-

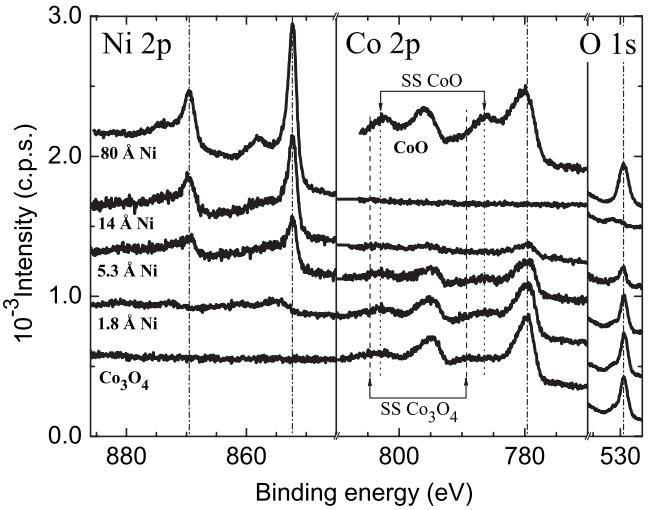

FIG. 5. X-ray photoelectron spectra of the $Ni/Co_3O_4(011)$ structure for different values of the Ni film thickness at the O 1*s*, Co 2*p* and Ni 2*p* edges. Also shown are the Co 2*p* and O 1*s* spectra of the CoO(001) reference sample. Dashed-dotted lines indicate the positions of the main O 1*s*, Co_3O_4, and Ni metal peaks; dotted lines show the positions of the satellite peaks of CoO and dashed lines the satellite energy positions of Co_3O_4. (Data have been shifted vertically for convenient display.)

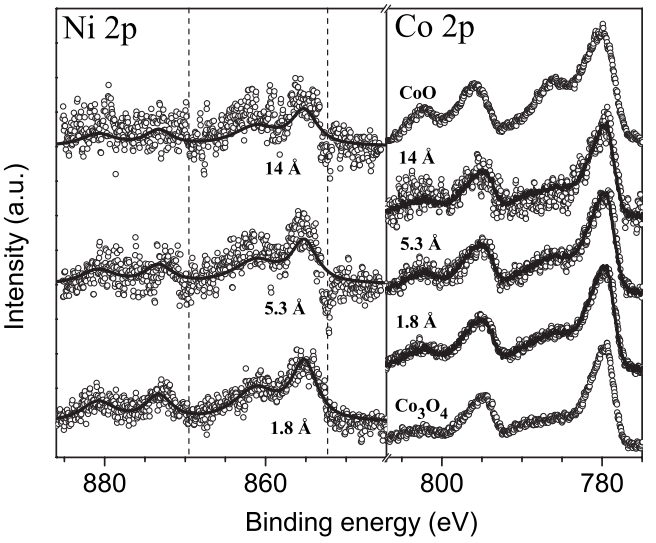

FIG. 6. Left panel: Ni 2*p* spectra of the 1.8 Å Ni film (original data) and for the 5.3 and 14 Å Ni films after removing the metallic Ni component; data are shown as circles, full lines are guides to the eyes, and dashed lines indicate the position of the metal Ni 2*p* main lines. Right panel: normalized Co 2*p* spectra (circles) and least-squares fits to linear combinations of the CoO and Co_3O_4 Co 2*p* spectra (full lines). Data have been shifted vertically for convenient display.

sorbed hydroxyl groups that also give rise to a similar feature.[72,73] Focusing first on the Co 2*p* spectra, we find a significant modification of the spectra between the 0 and 1.8 Å Ni film thicknesses; the spectrum of the 1.8 Å film exhibits a significant broadening of the main peaks and the presence of prominent satellite peaks at binding energies lower than those characteristic of Co_3O_4; indeed, comparison with the reference CoO spectrum indicates that these are characteristic of CoO. The conclusion is that a reduction in the Co_3O_4 surface has occurred, leading to the presence of a CoO-like interface layer. The same features persist at 5.3 and 14 Å Ni thicknesses. The Ni 2*p* spectra are also revealing. The 1.8 Å Ni film spectrum exhibits strong main lines that are shifted to higher binding energies with strong satellite peaks characteristic of Ni^{2+},[64] which also persist up to 14 Å Ni, although a strong metallic component develops in tandem.

Figure 6 shows a more detailed view of the Ni 2*p* and Co 2*p* spectra for the different Ni film thicknesses, where a linear background was subtracted from the data. The 1.8 Å Ni spectra is the same as in Fig. 5, plotted on an expanded scale. One striking observation is the presence of strong satellite peaks at 6.0 and 7.6 eV above the main peaks; the corresponding values for NiO lie at 7.3 eV and 8.2 eV, respectively.[74] Those differences are well beyond the experimental uncertainty; the observed satellite peak positions agree well with those for $NiCo_2O_4$, 6.4 eV and 7.5 eV, respectively,[66] which may be attributed to the altered electronic environment of the Ni cations or to the presence of a $NiCo_2O_4$ interfacial layer. For the 5.3 and 14 Å Ni 2*p* spectra, we use the fact that the metallic Ni $2p_{3/2}$ peak is well separated from the oxide Ni peak to subtract the metal Ni contribution from the 5.3 and 14 Å Ni XPS spectra, using the scaled 80 Å Ni spectrum as the reference. The remaining signal is attributed to the Ni^{2+} contribution; despite the low signal-to-noise ratio, the spectra are found to have features similar to the 1.8 Å Ni spectrum. To guide the eyes, we have superimposed on the data the result of a multipeak fit to the 1.8 Å Ni spectrum. The noise in the data precludes a quantitative estimate of the Ni oxide layer but the attenuation in the Ni-oxide signal with increasing thickness indicates that the Ni oxidation is confined to the interface, to within 2–4 Å or 1–2 atomic layers.

The Co 2*p* spectra shown in Fig. 6 are normalized to the $2p_{3/2}$ peak, which removes the attenuation from the Ni overlayer. In both this case and in that of the 2*p* Ni metal peak, the scaling factors follow an exponential decay, with an attenuation length (λ) of about 11 Å, which agrees with the tabulated effective attenuation lengths for the Co $2p_{3/2}$ and Ni $2p_{3/2}$ lines in Ni for our measurement geometry.[75] For the Co 2*p* lines, we attempt to estimate the thickness of the CoO layer by assuming that the Co 2*p* spectra of the 1.8, 5.3, and 14 Å Ni thicknesses can be described by a superposition of the Co_3O_4 and CoO bulk spectra, $I_0 = \alpha I_{CoO} + \beta I_{Co_3O_4}$. The resulting fits using least squares are shown as continuous lines in Fig. 6. We find $\alpha = 0.28(1)$, $\beta = 0.75(1)$ for the 1.8 Å Ni film; $\alpha = 0.30(2)$, $\beta = 0.69(2)$ for the 5.3 Å Ni film; and $\alpha = 0.11(3)$, $\beta = 0.81(3)$ for the 14 Å film, where the error bars correspond to three standard deviations. To first approximation, the scaled Co 2*p* XPS signal, $I_0 = I \exp\{+t_{Ni}/\lambda_{Ni}\}$ (where I is the measured intensity), is the sum of the signals originating from the CoO and the thick Co_3O_4 layers, $I_0 = I_\infty(1 - \exp\{-t_{CoO}/\lambda\}) + I_\infty \exp\{-t_{CoO}/\lambda\}$, assuming similar effective attenuation lengths and bulk intensities for the two Co oxides. The intensity should be therefore approximately

independent of the Ni film thickness, with $\alpha+\beta\approx 1$, in reasonable agreement with the fitting results given the approximations made. For the 14 Å Ni film, the agreement is less good, although the fit is also less satisfactory due to the larger scatter in the data. (Since the signal in this case weighs the interface region more strongly, one other possibility may be the presence of a $NiCo_2O_4$ interfacial layer; the latter is characterized by a Co $2p$ edge spectrum with strongly suppressed satellite peaks from the Co^{3+} cations occupying an octahedral environment,[66,76] which would resemble the Co_3O_4 spectrum more closely.) Using $\alpha=0.3$, we estimate $t_{CoO}\approx 4$ Å, using $\lambda=11$ Å. The extent of the Co_3O_4 reduction may also be deduced from the oxygen intake from the Ni interfacial layer according to $Ni+Co_3O_4\rightarrow NiO+3CoO$. Using a Ni atomic surface density similar to that of the Co^{3+} density in $Co_3O_4(110)$, and a Ni oxidation of 1–2 atomic layers, this results in the formation of 3–6 CoO molecules into the cobalt-oxide film, corresponding approximately to a thickness of 4.5–9 Å, using the (110) interplanar distance of 1.48 Å for CoO, in reasonable agreement with the estimate obtained from the XPS data.

Based on the XPS results, we can therefore rule out a pristine Ni/Co_3O_4 interface, and one must conclude that the exchange-bias effect observed in this system is not intrinsic to Co_3O_4. In fact, interfacial modifications in the oxidation state of CoO and NiO in contact with $3d$ ferromagnetic metals are also known to occur[10,77–80] while changes in the oxygen stoichiometry of CoO has also been found to have a marked influence on the exchange bias of Fe/CoO couples.[81] Two possible effects could contribute to the exchange anisotropy observed in Ni/Co_3O_4. One effect refers to the presence of the CoO layer, which has a bulk Néel temperature of 290 K.[16–21] Since the CoO layer remains relatively thin (~4 Å), the Néel temperature is depressed[82–84] but would otherwise give rise to large exchange bias at low temperatures; the largest exchange-bias effects reported in the literature have been observed for CoO.[4] The other effect results from the presence of the nickel interfacial oxide layer. $Ni_xCo_{1-x}O$ is antiferromagnetic with a critical temperature that varies linearly with x between that of CoO and NiO, well above that of cobaltite.[85] Since the exchange-bias effect is an interfacial effect, this layer must necessarily mediate the exchange coupling between the CoO and the Ni film. Despite its small thickness, it is likely to be magnetically polarized from contact with the Ni and the CoO layers. Both effects are consistent with the observation of exchange bias in Ni/Co_3O_4 at temperatures well above the Néel temperature of Co_3O_4.

IV. CONCLUSIONS

In conclusion, we have carried out a detailed study of the exchange bias and of the interfacial structure in $Ni/Co_3O_4(011)$. The exchange anisotropy is large, persists to temperatures well above the Néel temperature of bulk Co_3O_4, and is larger for the rougher Co_3O_4 films. From photoelectron spectroscopy carried out as a function of the Ni film thickness, the oxidation state of the Co_3O_4 and Ni films are found to be strongly modified at the interface, leading to the formation of a ~4 Å CoO layer and of a monolayer thick interfacial NiO layer. Such modifications in the interfacial oxidation state and electronic structure are difficult to assess with structural characterization techniques alone. We attribute the unusual exchange-bias behavior found in Ni/Co_3O_4 and similar metal/Co_3O_4 structures to the presence of such a modified interface. These results emphasize how interfacial reactions play a strong role in governing exchange bias and thus how detailed knowledge of the interfacial structure and electronic properties are essential to understanding these phenomena.

ACKNOWLEDGMENTS

The authors acknowledge financial support by the NSF through Grant No. MRSEC DMR 0520495 (CRISP).

*Corresponding author; carlos.vaz@cantab.net

[1] W. H. Meiklejohn and C. P. Bean, Phys. Rev. **102**, 1413 (1956).
[2] W. H. Meiklejohn, J. Appl. Phys. **33**, 1328 (1962).
[3] A. E. Berkowitz and K. Takano, J. Magn. Magn. Mater. **200**, 552 (1999).
[4] J. Nogués and I. K. Schuller, J. Magn. Magn. Mater. **192**, 203 (1999).
[5] R. L. Stamps, J. Phys. D **33**, R247 (2000).
[6] M. Kiwi, J. Magn. Magn. Mater. **234**, 584 (2001).
[7] C. Binek, *Ising-type Antiferromagnets*, Springer Tracts in Modern Physics Vol. 196 (Springer-Verlag, Berlin, 2003).
[8] F. Radu and H. Zabel, in *Magnetic Heterostructures*, Springer Tracts in Modern Physics Vol. 227, edited by H. Zabel and S. D. Bader (Springer-Verlag, Berlin, 2007), p. 97.
[9] I. Schmid, P. Kappenberger, O. Hellwig, M. J. Carey, E. E. Fullerton, and H. J. Hug, EPL **81**, 17001 (2008).
[10] H. Ohldag, T. J. Regan, J. Stöhr, A. Scholl, F. Nolting, J. Lüning, C. Stamm, S. Anders, and R. L. White, Phys. Rev. Lett. **87**, 247201 (2001).
[11] H. Ohldag, A. Scholl, F. Nolting, E. Arenholz, S. Maat, A. T. Young, M. Carey, and J. Stöhr, Phys. Rev. Lett. **91**, 017203 (2003).
[12] J. P. Picard, G. Baud, J. P. Besse, and R. Chevalier, J. Less-Common Met. **75**, 99 (1980).
[13] *Handbook of Chemistry and Physics*, 87th ed., edited by D. R. Lide (CRC Press, Boca Raton, 2006).
[14] W. L. Roth, J. Phys. Chem. Solids **25**, 1 (1964).
[15] D. Scheerlinck and S. Hautecler, Phys. Status Solidi B **73**, 223 (1976).
[16] H. Bizette, Ann. Phys. 12e Ser. **1**, 233 (1946).
[17] H. Bizette, J. Phys. Radium **12**, 161 (1951).
[18] C. H. La Blanchetais, J. Phys. Radium **12**, 765 (1951).
[19] W. L. Roth, Phys. Rev. **110**, 1333 (1958).
[20] C. G. Shull, W. A. Strauser, and E. O. Wollan, Phys. Rev. **83**,

333 (1951).
[21] W. Jauch, M. Reehuis, H. J. Bleif, F. Kubanek, and P. Pattison, Phys. Rev. B **64**, 052102 (2001).
[22] C. A. F. Vaz, Surf. Sci. **603**, 291 (2009).
[23] K.-W. Lin, F.-T. Lin, and Y.-M. Tzeng, Jpn. J. Appl. Phys. **44**, 3932 (2005).
[24] K.-W. Lin, F.-T. Lin, Y.-M. Tzeng, and Z.-Y. Guo, Eur. Phys. J. B **45**, 237 (2005).
[25] J. van Lierop, K.-W. Lin, Z.-Y. Guo, and B. W. Southern, J. Appl. Phys. **99**, 08C101 (2006).
[26] J. van Lierop, K.-W. Lin, J.-Y. Guo, H. Ouyang, and B. W. Southern, Phys. Rev. B **75**, 134409 (2007).
[27] T. B. Reed, *Free Energy of Formation of Binary Compounds* (The MIT Press, Cambridge, MA, 1971).
[28] P. H. Holloway, J. Vac. Sci. Technol. **18**, 653 (1981).
[29] B. D. Zion, A. T. Hanbicki, and S. J. Sibener, Surf. Sci. **417**, L1154 (1998).
[30] T. Okazawa, T. Nishizawa, T. Nishimura, and Y. Kido, Phys. Rev. B **75**, 033413 (2007).
[31] S. Song and F. Placido, Proc. SPIE **7101**, 710120 (2008).
[32] C. A. F. Vaz, V. E. Henrich, C. H. Ahn, and E. I. Altman, J. Cryst. Growth **311**, 2648 (2009).
[33] H. P. Tripp and B. W. King, J. Am. Ceram. Soc. **38**, 432 (1955).
[34] K. Koumoto and H. Yanagida, Jpn. J. Appl. Phys. **20**, 445 (1981).
[35] M. Oku and Y. Sato, Appl. Surf. Sci. **55**, 37 (1992).
[36] R. Jansen, V. A. M. Brabers, and H. van Kempen, Surf. Sci. **328**, 237 (1995).
[37] Y. Oda, S. Mizuno, S. Todo, E. Torikai, and K. Hayakawa, Jpn. J. Appl. Phys. **37**, 4518 (1998).
[38] G. Maris, O. Shklyarevskii, L. Jdira, J. G. H. Hermsen, and S. Speller, Surf. Sci. **600**, 5084 (2006).
[39] J. F. Anderson, M. Kuhn, U. Diebold, K. Shaw, P. Stoyanov, and D. Lind, Phys. Rev. B **56**, 9902 (1997).
[40] S. F. Ceballos, G. Mariotto, K. Jordan, S. Murphy, C. Seoighe, and I. V. Shvets, Surf. Sci. **548**, 106 (2004).
[41] M. B. Stearns, in *Magnetic Properties of Metals*, Landolt-Börnstein, New Series, Group III Vol. 19, Pt. A, edited by H. P. J. Wijn (Springer-Verlag, Berlin, 1986), p. 24.
[42] A. G. Every and A. K. McCurdy, in *Low Frequency Properties of Dielectric Crystals*, Landolt-Börnstein, New Series, Group III Vol. 29, Pt. A, edited by D. F. Nelson (Springer-Verlag, Berlin, 1992), p. 1.
[43] C. A. F. Vaz, J. A. C. Bland, and G. Lauhoff, Rep. Prog. Phys. **71**, 056501 (2008).
[44] T. J. Moran, J. M. Gallego, and I. K. Schuller, J. Appl. Phys. **78**, 1887 (1995).
[45] S. Kuriki and G. Matsumoto, J. Phys. Soc. Jpn. **35**, 304 (1973).
[46] S. Kuriki, J. Phys. Soc. Jpn. **40**, 44 (1976).
[47] S. Kuriki, IEEE Trans. Magn. **12**, 107 (1976).
[48] *Handbook of Chemistry and Physics*, 76th ed., edited by D. R. Lide (CRC Press, Boca Raton, 1995).
[49] H. P. J. Wijn, *Magnetic Properties of Metals: d-elements, Alloys and Compounds*, Data in Science and Technology (Springer-Verlag, Berlin, 1991).
[50] E. Schlömann, J. Appl. Phys. **41**, 1617 (1970).
[51] E. Schlömann and R. I. Joseph, J. Appl. Phys. **41**, 1336 (1970).
[52] P. Bruno, J. Phys. F: Met. Phys. **18**, 1291 (1988).
[53] P. Bruno, J. Appl. Phys. **64**, 3153 (1988).
[54] R. Arias and D. L. Mills, Phys. Rev. B **59**, 11871 (1999).
[55] J. H. Wolfe, R. K. Kawakami, W. L. Ling, Z. Q. Qiu, R. Arias, and D. L. Mills, J. Magn. Magn. Mater. **232**, 36 (2001).
[56] C. A. F. Vaz, S. J. Steinmuller, and J. A. C. Bland, Phys. Rev. B **75**, 132402 (2007).
[57] Y. Wang, B. You, W. Tian, Y. Wang, L. Sun, and M. Lu, Int. J. Mod. Phys. B **19**, 2580 (2005).
[58] Y. Wang, W. Tian, Y. Wang, L. Sun, Q. Li, B. You, A. Hu, H. Zhai, and M. Lu, Solid State Commun. **135**, 725 (2005).
[59] Y. Wang, Y. Zhang, Y. Cao, M. Lu, and J. Yang, J. Alloys Compd. **450**, 128 (2008).
[60] T. J. Chuang, C. R. Brundle, and D. W. Rice, Surf. Sci. **59**, 413 (1976).
[61] G. A. Carson, M. H. Nassir, and M. A. Langell, J. Vac. Sci. Technol. A **14**, 1637 (1996).
[62] S. C. Petitto and M. A. Langell, J. Vac. Sci. Technol. A **22**, 1690 (2004).
[63] C. R. Brundle, T. J. Chuang, and D. W. Rice, Surf. Sci. **60**, 286 (1976).
[64] K. W. Wulser and M. A. Langell, Catal. Lett. **15**, 39 (1992).
[65] Y. E. Roginskaya, O. V. Morozova, E. N. Lubnin, Y. E. Ulitina, G. V. Lopukhova, and S. Trasatti, Langmuir **13**, 4621 (1997).
[66] J.-G. Kim, D. L. Pugmire, D. Battaglia, and M. A. Langell, Appl. Surf. Sci. **165**, 70 (2000).
[67] Y. Jugnet and T. M. Duc, J. Phys. Chem. Solids **40**, 29 (1979).
[68] Y. M. Kolotyrkin, I. D. Belova, Y. E. Roginskaya, V. B. Kozhevnikov, D. S. Zakhar'in, and Y. N. Venevtsev, Mater. Chem. Phys. **11**, 29 (1984).
[69] B. Klingenberg, F. Grellner, D. Borgmann, and G. Wedler, Surf. Sci. **296**, 374 (1993).
[70] F. Grellner, B. Klingenberg, D. Borgmann, and G. Wedler, J. Electron Spectrosc. Relat. Phenom. **71**, 107 (1995).
[71] V. M. Jiménez, A. Fernández, J. P. Espinós, and A. R. González-Elipe, J. Electron Spectrosc. Relat. Phenom. **71**, 61 (1995).
[72] S. C. Petitto, E. M. Marsh, G. A. Carson, and M. A. Langell, J. Mol. Catal. A: Chem. **281**, 49 (2008).
[73] J. Haber and L. Ungier, J. Electron Spectrosc. Relat. Phenom. **12**, 305 (1977).
[74] R. P. Furstenau and M. A. Langell, Surf. Sci. **159**, 108 (1985).
[75] C. J. Powell and A. Jablonski, *NIST Electron Effective-attenuation-length database—Version 1.2* (National Institute of Standards and Technology, Gaithersburg, MD, 2009).
[76] C. A. F. Vaz, D. Prabhakaran, E. I. Altman, and V. E. Henrich, Phys. Rev. B **80**, 155457 (2009).
[77] T. J. Regan, H. Ohldag, C. Stamm, F. Nolting, J. Lüning, J. Stöhr, and R. L. White, Phys. Rev. B **64**, 214422 (2001).
[78] G. H. Yu, C. L. Chai, F. W. Zhu, J. M. Xiao, and W. Y. Lai, Appl. Phys. Lett. **78**, 1706 (2001).
[79] C. Tusche, H. L. Meyerheim, F. U. Hillebrecht, and J. Kirschner, Phys. Rev. B **73**, 125401 (2006).
[80] F. Allegretti, G. Parteder, M. G. Ramsey, S. Surnev, and F. P. Netzer, Surf. Sci. **601**, L73 (2007).
[81] G. Nowak, A. Remhof, F. Radu, A. Nefedov, H.-W. Becker, and H. Zabel, Phys. Rev. B **75**, 174405 (2007).
[82] T. Ambrose and C. L. Chien, J. Appl. Phys. **79**, 5920 (1996).
[83] D. Alders, L. H. Tjeng, F. C. Voogt, T. Hibma, G. A. Sawatzky, C. T. Chen, J. Vogel, M. Sacchi, and S. Iacobucci, Phys. Rev. B **57**, 11623 (1998).
[84] J. Keller, P. Miltényi, B. Beschoten, G. Güntherodt, U. Nowak, and K. D. Usadel, Phys. Rev. B **66**, 014431 (2002).
[85] P. Bracconi, J. Magn. Magn. Mater. **40**, 37 (1983).